RSC Advances

ROYAL SOCIETY OF CHEMISTRY

www.rsc.org/advances

Cite this: DOI: 10.1039/c0xx00000x

www.rsc.org/xxxxxx

ARTICLE TYPE

In situ observations of Pt nanoparticles coalescing inside carbon nanotubes

Magdalena Ola Cichocka [a,b], Jiong Zhao [a], Alicja Bachmatiuk [a,c,d], Huy Ta Quang [a,b], Sandeep M. Gorantla [d], Ignacio G. Gonzalez-Martinez [d,e], Lei Fu [f], Jürgen Eckert [d,e], Jamie H. Warner [g] and Mark H. Rümmeli*[a,b]

Received (in XXX, XXX) Xth XXXXXXXXX 20XX, Accepted Xth XXXXXXXXX 20XX
DOI: 10.1039/b000000x

In this in situ study, details of the coalescence of Pt nanoparticles encapsulated within carbon nanotubes are investigated whilst under electron irradiation in aberration corrected transmission electron microscopy. Coalescence occurs via the direct attachment of atoms on the surface, particle reorientation and relaxation.

Metal filled carbon nanotubes are receiving increasing attention because of their potential application in catalysis [1], and electronic devices [2,3]. Moreover, the structural, and chemical properties of metals inside CNTs are often different as compared to their counterparts in bulk form or when deposited on the outer walls of CNT [4]. For example, γ-Fe nanoparticles (NPs) with a face centered cubic (fcc) crystal structure are known to be stable between 1185-1667 K, yet inside CNTs their stability is retained even at room temperature [5]. Confined cobalt nanorods in CNTs show an fcc structure instead of the stable bulk hexagonal structure [6]. Previous research shows that platinum in the bulk form can adopt a (111) plane, which is the energetically-favorable growth plane of Pt films. Pt (111) facets have excellent structural and thermal stabilities [7]. Moreover, metal NPs inside CNTs usually show better catalytic performance than those on the outer surface [1,6,8]. An example can be platinum NPs encapsulated within CNTs [9]. Pt filled CNTs (Pt@CNTs) can show higher hydrogenation activity, enantioselectivity and average turnover frequency than CNT with surfaces decorated with Pt NPs.

It is important to stabilize nanoparticles that serve as catalysts, because coalescence is the main cause of their catalytic deactivation [10]. Pt nanoparticle coalescence has been investigated through various in-situ studies [10,11,12,13]. Oxygen -induced sintering on a planar, amorphous Al_2O_3 substrate has shown that Pt nanoparticles can adopt size-dependent morphologies after sintering. [10]. Previous work on the thermal stability of Pt nanoparticles on a graphene layer revealed that Pt nanoparticles and single atoms can anchor to the edge of the graphene layer, but some Pt atoms can migrate on the graphene surface [11] Coalescence of Pt NPs led by electron-excitation on amorphous graphene has been observed. They found that electron excitation can significantly enhance the van der Waals interaction between Pt nanoparticles and reduce the binding energy between Pt nanoparticles and the carbon substrate, both of which promote coalescence [12]. Exploring the mechanism of colloidal Pt nanocrystals growth via coalescence in an aqueous environment revealed that most coalescence processes proceed along the same crystallographic direction ((111) plane) and there is structural reshaping after coalescence, and surface faceting [13]. However the details of these process in a confined environment, e.g. inside a CNT have not yet been explored. Here, we present an in-situ study of Pt nanoparticles inside carbon nanotubes using Cs aberration corrected TEM at 80 kV. The confined environment of the CNT restricts the freedom of movement for the Pt nanoparticles leading to different coalescence behavior compared to non-confined reactions. In addition, we find many Pt nanoparticles have their (111) plane parallel to the tube wall which might suggest preferential alignment.

CNTs are vapor filled with Pt for our situ TEM study. After the capillary filling process, many of the CNT are decorated with Pt clusters on their outer wall or in some cases Pt NPs are encapsulated within (Fig. 1A).

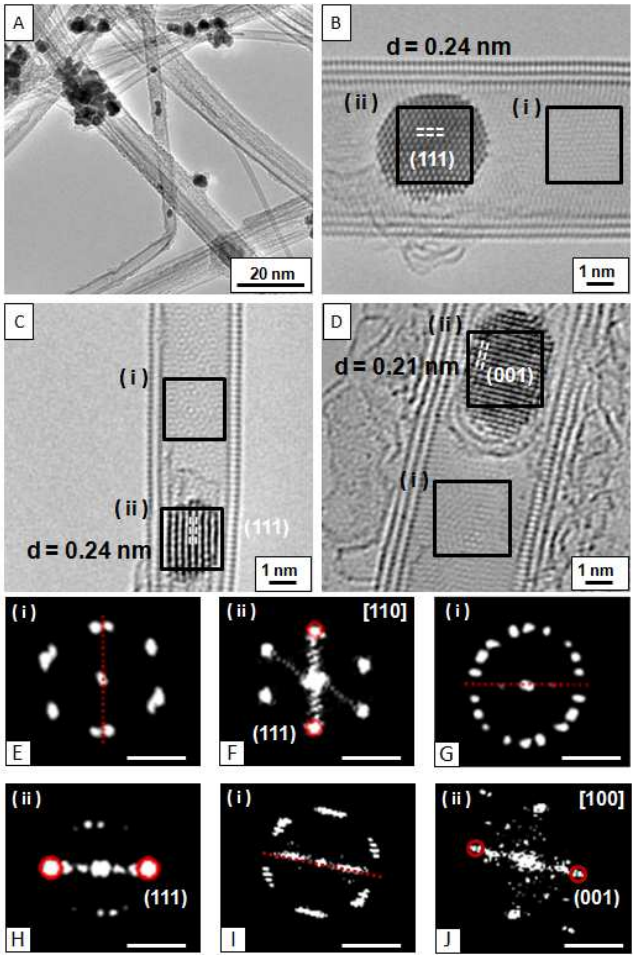

Fig. 1. (A) Low-magnification TEM image of Pt/CNTs (in and out) showing surface decoration with Pt NPs. In figure (B), (C) single crystal particles encapsulated within CNT have (111) faces parallel to the CNT wall. In figure (D) the Pt NP its (001) plane parallel to the CNT axis (zigzag configuration). Panels (E) to (J) are FFTs from from (B) to (D) respectively. The scale bar for panels (E) to (J) is 5 1/nm.

A Fast Fourier Transform (FFT) was applied to the HRTEM images in Fig. 1B to 1D of the Pt clusters to confirm the FCC Pt structure. Statistical analysis of the images show that most of the CNTs have 2 to 4 walls as shown in Fig. S1A and around 20% of the tubes are filled with Pt clusters (Fig. S1B).

Many of the Pt nanocrystals inside CNTs have their (111) plane parallel to the CNT wall e.g. Fig. 1B,C, Fig. S1C, hinting preferential alignment may occur. Statistical studies show that ~ 36 % of all single crystalline Pt nanoparticles which are too large to rotate within their host CNT have their (111) plane parallel to the CNT long axis. In cases where the encapsulated single crystalline particles can rotate approximately 30% of them have their (111) plane parallel to the CNT axis. Furthermore a number of polycrystalline particles are observed. Of these, for particles which can rotate only ca. 5% have a (111) face parallel to the CNT walls while for those particles which cannot rotate only 2% had (111) faces parallel to the CNT walls (Fig. S1). The polycrystalline structures are in essence twinned structures, most of which show multiple twinning. Examples are provided in Figs. 2 A-D and Fig. S1D.

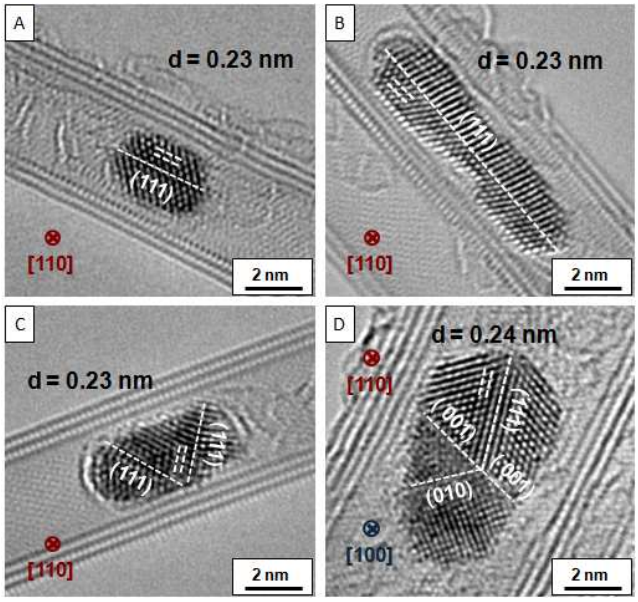

Fig. 2. Examples of twinned Pt nanoparticles encapsulated within CNT.

We now turn to the behavior of encapsulated Pt nanoparticles whilst under extended electron beam irradiation, in particular, the coalescence process of these particles. In figure 3, the first row of micrographs (Fig. 3A-C) show the beginning of crystallization and the alignment processes of the crystal planes for two merging particles. Initially the two attached nanoparticles have two different zone axis of [111] and [100]. The insets show magnifications of the merging regions from panels A to C. They show that the lower particle rotates in the clockwise direction and moves upwards. The lower particle also changes its zone axis from [100] to [111]. A 15° rotation is necessary to do this and, thus, the mismatch between these two particles is decreased. The neck between the two particles reconstructs by two mechanisms, atom by atom migration along the edge of the Pt nanoparticle and rotation of the whole particle. Atom movement on the Pt surface is driven by energy from the electron beam which allows the necking region (concave areas on surface) to be filled. The inset from Fig. 3B, shows an edge dislocation appears at the necking position. This dislocation then disappears (see inset in panel C). The formation and

annihilation of dislocations shows plastic deformation at the necking area during the coalescence process. Moreover in Fig. 3B one can see a twinning plane between the merging particles (indicated with an arrow) which starts to disappear with extended irradiation (Fig. 3C) as the (101) planes in each particle start to align with each other.

The second row of micrographs in Fig. 3 (Fig. 3D-F) shows the complete electron beam induced crystallization process which results in a single crystalline Pt particle after a single-crystal Pt particle coalesces with a multi-twinned particle. The bright contrast area in the middle is where the merging occurs (Fig. 3D).

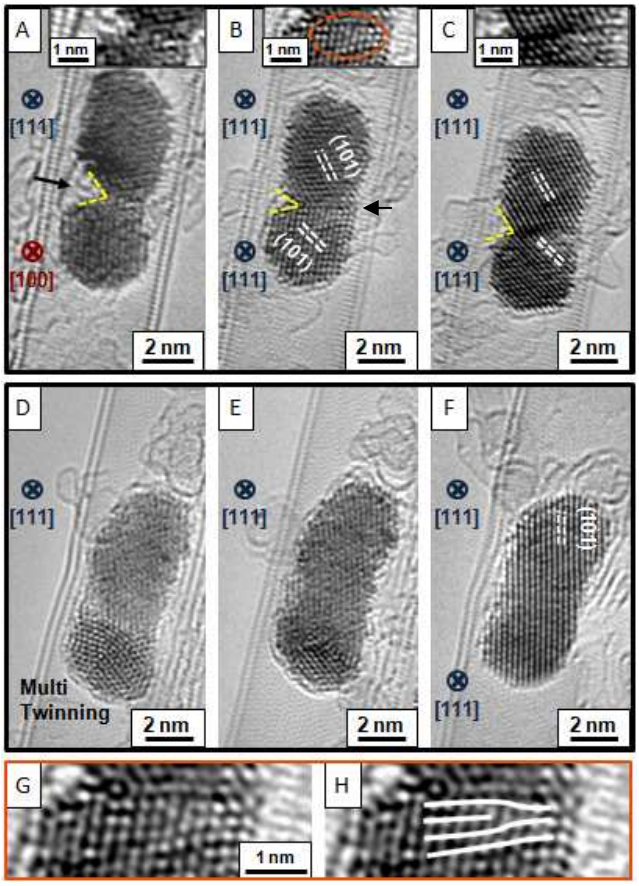

Fig. 3. Two examples of the coalescence process between two Pt particles (A-C and D-F). Panels G and H are magnifications of the necking regions from panel B to highlight the presence of a dislocation. Arrow in A indicates necking region and arrow in B indicates twinning plane.

Figure 4 shows a more detailed examination of the coalescence process. The images were sequentially with 60 seconds between each frame and selected images are provided in figure 4. The full process can be observed in the movie in the supplementary information. The micrographs clearly demonstrate atomic mobility under electron beam irradiation which is due to the transfer of kinetic energy from the high energy electrons from the imaging beam to the Pt atoms (A calculation of the temperature rise (ΔT) of Pt nanoparticles due to electron beam irradiation show a temperature rise of less than 1 K. (See supplementary information S5)).

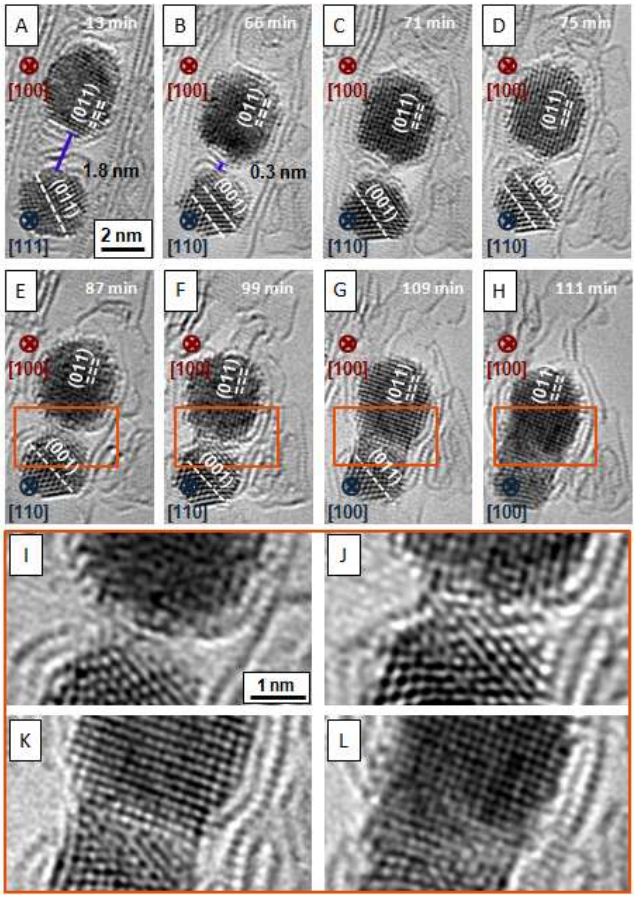

Fig. 4. TEM micrographs showing details of the in-situ coalescence of two Pt nanoparticles whilst under electron irradiation. Panels I to L show magnifications of the necking regions outlined with orange boxes in panels E to H.

The mobility of the surface atoms plays an important role in the coalescence of the Pt particles. Fig. 4A shows two Pt nanoparticles encapsulated in a CNT and surrounded by some amorphous carbon, which probably comes from the Pt precursor. The initial relative orientation between the two single crystal particles is different. Figs. 4A-C show the distance between the two nanoparticles gets smaller. Surface atoms between the two particles can migrate under electron beam irradiation as we have mentioned above. By the time we get to Fig. 4D and Fig 4E the lower nanoparticle is attached to the upper nanoparticle and a (disordered) necking region forms. The necking regions for panels E to H are magnified in panels I to L respectively. Continuous reconstructions in the lower particle under

electron beam irradiation can then be observed. The lower particle rotates by shearing, which causes twinning. Under continued irradiation, the connection between two nanoparticles can translocate, deform or collapse and thus reconstruct. Double twinning planes are then observed to shift downward so that a single twinning plane is left. Fig. 4F shows early coalescence. Two possible mechanisms mediate this process as the coalescing particles seek to minimize surface energy: shearing of the particle and atomic diffusion. A slight misalignment at the time of attachment can lead to different defects forming at the interface. Fig. 4G reveals the intermediate interaction process. The upper particle is swiftly rotated by 8°. The defect seems to disappear during the recrystallization process under electron beam irradiation. From the micrographs, the sintering area contains a semicrystalline region (Fig. 4F). A de-twinning process occurs before complete recrystallization (Fig. 4H). After the last frame (Fig. 4H) was captured, a significant portion of the CNT collapsed preventing capture of the final step of the coalescence process so as to form a single crystal as shown in Fig 3F.

The atomic rearrangement during the coalescence process seems to occur via dislocation dynamics and interface (including twinning plane and grain boundary) migration [14]. The energy stored in dislocations and twinning structures can also contribute to the energy needed for recrystallization. On the other hand, the reduction of surface energy constitutes the main driving force for the fusion process. Moreover there is also a reduction of the surface energy of the particles to achieve stable (111) facets with low curvature at the end.

Conclusions

In summary, we observe the coalescence of Pt nanoparticles inside few walled carbon nanotubes whilst under electron beam irradiation (with an 80 kV acceleration voltage) inside an aberration corrected TEM. Single nano-crystalline particles coalesce via direct attachment of atoms on the surface, particle reorientation and relaxation. The primary energy for driving the Pt nanoparticle coalescence comes from transferred electron energy from the imaging beam.

Notes and references

[a] *IBS Center for Integrated Nanostructure Physics, Institute for Basic Science (IBS), Daejon 305-701, Republic of Korea, E-mail: mark@rummeli.com*
[b] *Department of Energy Science, Department of Physics, Sungkyunkwan University, Suwon 440-746, Republic of Korea,*
[c] *Center of Polymer and Carbon Materials, Polish Academy of Sciences, M. Curie-Sklodowskiej 34, Zabrze 41-819, Poland*
[d] *IFW Dresden, Institute of Complex Materials, P.O. Box 270116, D-01171 Dresden, Germany*
[e] *Technical University (TU) Dresden, Institute of Materials Science, D-01062 Dresden, Germany*
[f] *College of Chemistry and Molecular Science, Wuhan University, 430072, China*
[g] *Department of Materials, University of Oxford, 16 Park Road, Oxford OX1 3PH, United Kingdom*

† Electronic Supplementary Information (ESI) available: [Sythesis procedure of the platinum filled carbon nanotubes. Statistics of the Pt nanoparticles morphology and orientation. Detailed in-situ TEM images of the coalescence process. EDS of the platinum filled carbon nanotubes. Estimation of the beam-induced temperature rise in the Pt nanoparticles. Explanation for spatial calibration. Movie of the coalescence Pt particles.]. See DOI: 10.1039/b000000x/

1 P Serp, E. Castillejos, *ChemCatChem*, 2010, **2**, 41-47;.
2 D.-M. Tang, L.Ch. Yin, F. Li, Ch. Liu, W.-J. Yu, P.-X. Hou, B. Wu, Y.-H. Lee, X.-L. Ma, H.-M. Cheng, *Proc. Natl. Acad. Sci. USA*, 2010, **107**, 9055-9059;
3 D. Golberg, P.M.F.J. Costa, M. Mitome, S. Hampel, D. Haase, Ch. Mueller, A. Leonhardt, Y. Bando, *Adv. Mater*., 2007, **19**, 1937-1942;
4 A. La Torre, M. del Carmen Gimenez-Lopez, M.W. Fay, G.A. Rance, W.A. Solomonsz, T.W. Chamberlain, P.D. Brown, A.N. Khlobystov, *ACS Nano*, 2012, **6(3)**, 2000-2007;
5 H. Kim, W. Sigmund, *Journal of Crystal Growth*, 2005, **276**, 594-605;
6 S. Liu, J. Zhu, Y. Mastai, I. Felner, A. Gedanken, *Chem. Mater*., 2000, **12**, 2205- 2211;
7 R Huang, Y.-H. Wen, Z.-Z. Zhu, S.-G. Sun, *J. Mater. Chem*., 2011, **21**, 11578-11584;
8 T.T. Nguyen, P. Serp, *ChemCatChem*, 2013, **5**, 3595-3603;
9 C. Mateo-Mateo, C. Vazquez-Vazquez, M. Perez-Lorezno, V. Salgueirino, M.A. Correa-Duarte, *Journal of Nanomaterials*, 2012, **2012**, 6 pages;
10 S.B. Simonsen, Ib. Chorhendorff, S. Dahl, M. Skoglundh, K. Meinander, T.N Jemsen, J.V. Lauritsen, S. Helveg, *The Journal of Physical Chemistry C*, 2012, **116**, 5646-5653;
11 A. Hashimoto, M. Takeguchi, *J. Electron Microsc.,* 2012, **61(6)**, 409-413;
12 Y. Jiang, Y. Wang, Y.Y Zhang, Z. Zhang, W. Yuan, Ch. Sun, X Wei, CN. Brodsky, Ch-K. Tsung, J. Li, X. Zhang, S.X. Mao, S. Zhang, Z. Zhan,. *Nano Research,* 2014, **7(3)**, 308-314.
13 J.M. Yuk, J. Park, P. Ericus, K. Kim, D.J. Hellebusch, M.F. Crommie, J.Y. Lee, A. Zettl, A.P. Alivisatos, 2012, *Science*, **336(6077)**, 61-64;
14 J.M. Yuk, M. Jeong, S.Y. Kim, H.K. Seo, J. Kim, J. Y. Lee, Chem. Commun., 2013, **49**, 11479-11481;
15 M.A. Asoro, D. Kovar, Y. Shao-Horn, L.F. Allard, PJ. Ferreira, *Nanotechnology*, 2010, **21**, 025701-025707;
16 P. Schapotschnikow, M.A. van Huis, H.W. Zandbergen, D. Vanmaekelbergh, T.J.H. Vlugt, *Nano Letters*, 2010, **10**, 3966-3971;
17 I.G. Gonzalez-Martinez, S.M. Gorantla, A. Bachmatiuk, V. Bezugly, J. Zhao, T. Gemming, J. Kunstmann, J. Eckert, G. Cuniberti, M.H. Rümmeli, *Nano Letters*, 2014, **14**, 799-805;
18 L.-C. Liu, S.H. Risbud, *J. Appl. Phys*. 1994, **76**,4576-4580;
19 L. Pages, E. Bertel, H. Joffre and L. Sklavenitis, *Atomic Data*, 1972, **4**, 1-127.

